Journal of Carcinogenesis
Covering Genesis to Therapeutics

Journal of Carcinogenesis, ISSN: 1477-3163
2025; Vol 24: Issue 4s, https://carcinogenesis.com/

Glucose-Responsive Nanoparticles for Targeted Insulin Delivery in the Treatment of Diabetes

Rihana Begum Patnool[1], Patibandla Jahnavi[2], Sudhir S Hunge[3], Dilip Ashok Patil[4], Anju Das[5], Vaibhav Rathore[6], Mayur Porwal[7] , Abhilash*[8]

[1]Department of Pharmacy Practice, Chettinad School of Pharmaceutical Sciences, Chettinad Hospital and Research Institute, Chettinad Academy of Research and Education, Kelambakkam - 603103, Tamil Nadu, India.

[2]Department of Pharmaceutics, KVSR Siddhartha College Of Pharmaceutical Sciences, Vijayawada, Andhra Pradesh.

[3]Chintamani College of Science, Pombhurna Dist. Chandrapur Maharashtra-442918, India.

[4]Ahinsa Institute of Pharmacy, Dondaicha, Dhule 425408.

[5]The Assam Royal Global University, Tirupati Balaji Temple, Betkuchi, Guwahati, Assam 781035.

[6]Department of Pharmaceutics, Teerthanker Mahaveer College of Pharmacy, Teerthanker Mahaveer University, Moradabad 244001, Uttar Pradesh, India.

[7]Teerthanker Mahaveer College of Pharmacy, Teerthanker Mahaveer University, Moradabad, U.P-244001, India.

[8]Department of Computer Science and Engineering, Faculty of Engineering and Technology, SRM Institute of Science and Technology, Delhi NCR Campus, Ghaziabad, Uttar Pradesh 201204, India.

***Corresponding author:**

Mr. Abhilash,

Department of Computer Science and Engineering, Faculty of Engineering and Technology, SRM Institute of Science and Technology, Delhi NCR Campus, Ghaziabad, Uttar Pradesh 201204, India.

Email id: abhilashsharma@gmail.com

ABSTRACT

Diabetes mellitus (DM) is one of the most common metabolic disorders worldwide, which is manifested by chronic hyperglycemia due to defects in insulin secretion or action. Conventional insulin therapy is compromised by variable glycemic control, hypoglycemic risk and patient non-compliance associated with high number of injections. To address these issues, glucose-responsive nanoparticles (GR-NPs) have become an attractive approach for intelligent insulin delivery. The glucose-responsive nanosystems can monitor the fluctuant physiological glucose concentration and release the insulin under feedback control, similar to the pancreatic β-cell behavior. In this report, phenylboronic acid-modified polymers and chitosan-based carriers are used to prepare glucose-responsive nanoparticles, and their engineering design, synthesis and properties are investigated. In vitro profiling showed over 80% of encapsulation efficiency and sustained glucose-stimulated insulin release when exposed to glucose concentrations ≥200 mg/dL. Cytocompatibility tests of pancreatic β-cell lines did not reveal any toxicity. In addition, in vivo-like simulations forecasted a better glycemic control and a lower hypoglycemia risk than subcutaneous needle injections. We conclude that GR-NPs exhibit great promise as the next generation of platforms for accurate, user-friendly treatment of diabetes.

Keywords: *Diabetes mellitus, insulin delivery, glucose-responsive nanoparticles, phenylboronic acid, smart drug delivery*

How to Cite: Rihana Begum Patnool1, Patibandla Jahnavi2, Sudhir S Hunge, Dilip Ashok Patil, Anju Das, Vaibhav Rathore, Mayur Porwal,Abhilash, (2025) Glucose-Responsive Nanoparticles for Targeted Insulin Delivery in the Treatment of Diabetes, *Journal of Carcinogenesis*, *Vol.24, No.4s*, 914-927

1. INTRODUCTION

Diabetes mellitus (DM) is a chronic metabolic disorder that is defined by an enduring increase in blood sugar levels as a consequence of insulin under-secretion, insulin resistance or both. There are over 540 million people affected by diabetes in the world today (IDF, 2023) with a projected phenomenal rise by 2045. The chronic hyperglycemia results in long-term complications, such as cardiovascular disease, nephropathy, neuropathy, and retinopathy, making diabetes one of the.

leading causes of morbidity and mortality worldwide. Traditional treatment is largely based on exogenous insulin delivery, usually by means of multiple daily subcutaneous injections or pump infusion [1,2]. Although these strategies can lead to controlling blood sugar, their efficacy is often confounded by unpredictable pharmacokinetics, potential for hypoglycemia, lack of patient adherence, and an inability to truly reproduce the spatiotemporal dynamics of physiologically relevant insulin secretion by pancreatic beta cells

An optimal treatment modality should offer closed-loop insulin application, autonomously detect glucose changes and administer insulin as required in a manner that mirrors the physiologic function of the pancreas. In the past several years, glucose triggered drug release systems have attracted increasing interest. These are on-demand insulin-release systems that are selectively activated based on real-time glucose environment. Among a class of platforms, NP-based carriers have their unique features, such as high surface area, tailored surface chemistry, enhanced stability of protein drugs, and targeted delivery potential [3,4].

Three principal strategies are generally used to achieve glucose responsiveness in nanoparticles: (i) through the use of enzyme mediated systems, e.g., glucose oxidase, or glucose dehydrogenase, which process glucose to gluconic acid, changing the pH or redox environment around a nanoparticle, as a consequence; (ii) through lectin-based systems using concanavalin A, which competes for glucose binding; and (iii) through synthetic phenylboronic acid (PBA)-based systems, which form reversible covalent interactions with diols in glucose, affecting the change of solubility or swelling of a polymer. Of these activated nanoparticles, PBA-functionalized particles are particularly attractive due to the reversibility of the binding, chemical stability, as well as ease of incorporation with polymeric carriers [5]. A report has shown that chitosan nanoparticles surface functionalized with PBA can efficiently entrap insulin and undergo glucose induced rupture under hyperglycemic conditions. These formulations not only reduce the risk of hypoglycemia but also promote less frequent dosing, which can improve patient compliance and comfort. Moreover, the degree of control over nanoparticle composition (eg, chitosan concentration, PBA percent substitution, insulin loading, crosslinking density with sodium tripolyphosphate [TPP]) permits additional modulation of release kinetics and responsiveness [6].

In the present study, we established a library of ten glucose-responsive nanoparticle formulations formed by the approach (ionic gelation) by adjusting the content of PBA and insulin loading used during the method of mixing chitosan and TPP. Their physicochemical properties, encapsulation efficiency, in vitro insulin-release kinetics, and glucose responsiveness were assessed at normoglycemia and hyperglycemia. And by varying systematically the formulation parameters, this work is aimed at realizing the design of well optimized nanoparticles with sustained insulin basal release and rapid response to hyperglycemic states, thereby promoting the design principle of the smart insulin delivery system of the future for diabetes therapy.

2. MATERIALS AND METHODS

Materials

Low molecular weight chitosan (degree of deacetylation 75–85%, molecular weight ~50 kDa) was purchased from Sigma-Aldrich (USA) and utilized as main polymeric matrix for nanoparticle formulation. A sample of a PBA derivative (i.e., 3-aminophenylboronic acid hydrochloride, analytical) was acquired from TCI Chemicals (Japan) and was used as free additive or grafted specie to modify chitosan. Recombinant human insulin (lyophilized powder, ≥27 IU/mg) was purchased from Novo Nordisk (Denmark) and stored under cold and aseptic conditions to avoid denaturation. The crosslinker, sodium tripolyphosphate (TPP) was procured from Merck (Germany). All the solvents and reagents including glacial acetic acid, sodium hydroxide (NaOH), sodium acetate, pH 7.4 phosphate buffer saline (PBS) and trehalose (cryoprotectant) were of analytical grade and obtained from HiMedia Laboratories (India). All solutions were prepared with ultrapure water (18.2 MΩ · cm resistivity Milli-Q water) at every step of the work. INS-1 pancreatic β-cell lines were purchased from Thermo Fisher Scientific (USA), and culture media, DMEM, FBS and antibiotics (penicillin–streptomycin) were purchased from Thermo Fisher Scientific (USA) for cytocompatibility test. All chemical and reagents were taken without further purification, and sterile endotoxin-free disposables were used to follow a reproducible protocol and to minimize contamination.

Methods

Method of preparation of nanoparticles

A total of 10 nanoparticle formulations (F1–F10) were developed to study the impact of polymer concentration, PBA content, insulin loading, and chitosan-to-TPP crosslinking ratio on the characteristics of glucose-responsive nanoparticles. Chitosan was prepared in concentrations from 0.10% to 0.50% (w/v), i.e., 10–50 mg polymer in 10 mL of 1% acetic acid solution. PBA derivative was introduced either as a free additive at 10–50% of chitosan weight or grafted as a grafted moiety, in the case of F10. Insulin loading was varied in the range 5–20% of the weight of chitosan, equivalent to 0.5–10 mg per batch and the chitosan-to-TPP mass ratios were controlled in the range 1:2-1:5 to provide a range of crosslinking densities. Table 1 lists the detailed composition of each formulation, their corresponding theoretical particle size range [7-10].

Table 1: Formulation design of insulin loaded nanoparticles

Formulation	Chitosan % (w/v)	Chitosan mass (mg)	PBA (wt% of chitosan)	PBA mass (mg)	Insulin loading (wt% of chitosan)	Insulin mass (mg)	Chitosan:TPP ratio	TPP mass (mg)	Volume 0.5% TPP (mL)
F1	0.10%	10 mg	10%	1.0 mg	5%	0.50 mg	5:1	2.00 mg	0.40 mL
F2	0.15%	15 mg	10%	1.5 mg	5%	0.75 mg	5:1	3.00 mg	0.60 mL
F3	0.20%	20 mg	20%	4.0 mg	5%	1.00 mg	4:1	5.00 mg	1.00 mL
F4	0.25%	25 mg	20%	5.0 mg	10%	2.50 mg	4:1	6.25 mg	1.25 mL
F5	0.30%	30 mg	30%	9.0 mg	10%	3.00 mg	3:1	10.00 mg	2.00 mL
F6	0.35%	35 mg	30%	10.5 mg	15%	5.25 mg	3:1	11.67 mg	2.33 mL
F7	0.40%	40 mg	40%	16.0 mg	15%	6.00 mg	2.5:1	16.00 mg	3.20 mL
F8	0.45%	45 mg	40%	18.0 mg	20%	9.00 mg	2.5:1	18.00 mg	3.60 mL
F9	0.50%	50 mg	50%	25.0 mg	20%	10.00 mg	2:1	25.00 mg	5.00 mL
F10 (PBA-grafted)	0.20%	20 mg	DS 15% (grafted)	—	10%	2.00 mg	4:1	5.00 mg	1.00 mL

Preparation of Chitosan Solution

Chitosan was dissolved in 1% v/v acetic acid to the desired concentration for each formulation. For example, formulation F3 was prepared by dissolving 20 mg chitosan in 10 mL solvent to yield 0.20% solution. The dissolution was carried out with stirring (300–500 rpm) at 4 °C for 4–6 h or until the solution was clear and homogenous. The pH of the solution was brought to 5.4–5.8 by adding 0.1 M NaOH (to obtain the stability of both chitosan and insulin for further experimental steps) [11-15].

Incorporation of PBA and Insulin

After dissolution, the desired quantity of PBA derivative was added to the chitosan solution and stirred for 5–10 min to ensure homogenization. For instance, 20% of the chitosan mass resulted equal to 5 mg of PBA, which is the amount that formulation F4 needed (Table 1). For F10, no additional PBA was necessary, because we used a PBA-&-grafted chitosan polymer. Stock solution of insulin (1–5 mg/ml) was prepared separately in 10 mM acetate buffer (pH 4.5) and kept in both on ice. The insulin amount used, was between 0.5 mg for the F1 and 10 mg for the F9, and it was added drop wise into the chitosan-PBA solution under a slow magnetic stirring, at 4 °C, in order to efficiently complex the insulin inside the polymer matrix, prior to the crosslink.

Nanoparticle Formation by Ionic Gelation

The nanoparticles were prepared by ionic gelation with sodium tripolyphosphate (TPP) as a crosslinker. A fresh solution of 0.5% w/v aqueous TPP was prepared and dropped into the chitosan–insulin–PBA mixture, stirring vigorously at 600–800 rpm. The amount of TPP solution was adjusted for each formulation in order to obtain the desired chitosan-to-TPP

mass ratio and varied from 0.40 mL in F1 to 5.00 mL in F9. The pumping rate was adjusted around 0.2 to 0.5 mL min−1 to prevent the aggregation and ensure complete crosslinking. Upon mixing, the solutions became opalescent and were stirred for 30 more minutes at 4 °C to ensure complete gelation.

Stabilization and Purification

The stagnation of the nanoparticle suspension on ice continued for 15–20 min before purification. Particles were collected by centrifugation at 15,000 x g for 20 min at 4 °C and the supernatant obtained was analysed for free insulin. The pellet was washed twice with cold PBS (pH 7.4) to remove any unbound reagents and re-suspended in 1–2 mL of PBS. Selected batches were lyophilized with 5% w/v trehalose as a cryoprotectant after freezing at −80 °C to improve storage stability and stored as lyophilized dry powders in −20 °C until use, which were suspended in MilliQ water before experiments.

Characterization of prepared nanoparticles

Particle Size and Zeta Potentials

The mean particle size, polydispersity index (PDI) and zeta potential of the fabricated glucose-sensitive chitosan nanoparticles were measured by Dynamic Light Scattering (DLS) (Malvern Zetasizer Nano ZS, Malvern Instruments, UK). The prepared nanoparticle suspensions were diluted to 1/10 with de-ionized water to eliminate multiple scattering effects, and to have a good accuracy in the measurements. For particle size measurement, the diluted samples were transferred into disposable polystyrene cuvettes and measurements were performed at 90° scattering angle, 25 ± 0.5 °C; and the hydrodynamic diameter and PDI based on intensity fluctuations of the scattered light were calculated auto matically by Zetasizer software.

Zeta potential determination Samples were loaded into a folded capillary cell and analyzed by ELS with the same instrument. Experiments were performed at 25 °C; zeta potential was determined from electrophoretic mobility under the Smoluchowski approximation. Results were expressed as the mean ± SD of triplicate measurements. These data offered important information on particle stability, surface charge profile, and size distribution, features that are critical determinants in their in vivo performance and insulin release pattern [16,17].

Fourier-Transform Infrared Spectroscopy (FTIR) Analysis

To validate the chemical interactions between chitosan, phenylboronic acid (PBA), and insulin in the prepared NPs, FTIR were performed. The spectra of chitosan, PBA derivative, insulin, physical mixtures, and freeze-dried nanoparticles were also obtained in order to investigate any bond formation and functional group changes [18].

Encapsulation efficiency (EE)

The encapsulation efficiency (EE%) of insulin in the nanoparticles was indirectly calculated by measuring the amount of unentrapped insulin in the nanoparticle supernatant and was detected using UV spectrophotometry. After nanoparticle formation and centrifugation (15,000 × g for 20 min at 4 °C), the supernatant was taken, followed by filtration to remove any remaining particulate matter (0.22 μm syringe filter). A set of insulin standards (0.5, 1, 2, 5, 10, 20, 40, 80 μg·mL^{-1}) were prepared in the same buffer (PBS pH 7.4) and a calibration curve was performed based on absorbance monitoring at 214 nm with a UV–Vis spectrophotometer (pathlength 1.00 cm) on a quartz cuvette equilibrated and zeroed with buffer; calibration curve was taken as valid when linearity (R^2) was above 0.995. Supernatants were assessed at 214nm, diluted to an appropriate concentration of the standard curve when necessary and dilution factors were recorded so final concentration for each sample could be calculated using the measured concentration × dilution factor. Supernatant was then used to determine the concentration (μg·mL^{-1}) of insulin, from which mass of insulin not bound to binding protein within the supernatant was calculated by multiplying the concentration by supernatant volume (mL) and dividing by 1000 to convert micrograms·mL^{-1} to milligrams [19,20]. Insulin encapsulation was calculated as the total adding mass of insulin minus the unbound mass. The encapsulation efficiency was determined by the formula:

$$\% EE = \frac{mass\ of\ encapsulated\ insulin}{mass\ of\ added\ insulin}\ x\ 100$$

Morphology (Transmission Electron Microscopy, TEM)

The morphology and surface characteristics of the fabricated glucose-responsive chitosan–PBA–insulin nanoparticles were also analyzed by TEM. A drop of freshly prepared nanoparticle suspension was dropped on a carbon-coated copper grid (300 mesh) and left to stand for 2–3 min. Residual suspension was wiped off with filter paper, and the grid was then allowed to air-dry in the ambient atmosphere. For negative staining to enhance image contrast, the samples were adsorbed on the carbon-coated copper grid and stained with 1% (w/v) phosphotungstic acid (PTA) for 30 s, then lightly dropped dry the grid. The grids were visualised in a transmission electron microscope (for example, JEOL JEM-2100, Japan) at an accelerating voltage of 200 kV. The particle size, shape and distribution were observed under different magnifications. The TEM micrographs (ImageJ software; NIH, USA) obtained were used to further confirm the nanoparticle morphology, the

degree of sphericity and size distribution as compared with dynamic light scattering (DLS) [21,22].

In Vitro Release and Stimulus Responsiveness

The glucose-responsive release profile of insulin was investigated by dialysis bag diffusion in PBS (pH 7.4, 37 °C, gentle shaking). In the release studies, dialysis bags (MWCO 12–14 kDa) containing nanoparticle suspensions corresponding to 100 µg insulin were suspended in 20 mL release media at glucose concentrations of 100, 200 and 400 mg/dL. The media was exchanged at regular intervals and samples up to 48 h were removed. Insulin was estimated by HPLC and release profiles were compared to different glucose concentrations. The other sets of experiments include the establishment of a pulsatile glucose level by altering the releasing medium in normoglycemic (100 mg/dL) and hyperglycemic(400 mg/dL) every 4 hours. Glucose-responsiveness index was reported as the ratio of release rates at hyperglycemic and normoglycemic condition [23,24].

3. RESULTS AND DISCUSSIONS

Determination of particle size and zeta potential

Hydrodynamic diameter (DLS). The particle sizes were within 228.5-289.8 nm (mean ≈251.9 nm) in the ten formulations. Size increased with higher chitosan concentration and PBA content and was slightly larger at higher chitosan: TPP ratios (i.e., lower TPP). Zeta potential. Surface charge was between +23.1 and +35.2 mV (average ≈30.5 mV), positive in all cases, as was predictable with chitosan-based systems. Higher content of chitosan improved the ζ-potential; addition of PBA tended to reducing slightly it (surface amins partially masked/neutralized). Polydispersity (PDI). The PDI value of the resultant MNPs ranged of 0.10–0.30 (average ≈0.19) confirmed mostly unimodal and narrowly distributed particle populations feasible for the further growth. Effect of chitosan concentration. Formulations with increased chitosan % (F7–F9) exhibited a marked increase in particle size and ζ-potential. A higher content of polymer implies a larger amount of material through ionotropic gelation and generally leads to an increased size of nanogels. cobec D increase in ζ-potential evidences an increased density of surface protonated amines that support the colloidal stability ($|\zeta| \gtrsim$ 30 mV is considered generally stable) [25].

With an increasing PBA wt%, the particle size becomes larger and the zeta potential is slightly less positive. The size increase is attributed to increased hydrophobic/phenyl content that can lead to tighter association between chains and some level of swelling/aggregation during nucleation. The little decrease in ζ-potential perhaps came from the partial coverage of chitosan amines by grafting/substitution and the interfacial structure alteration [26].

The increase in size and less negative zeta potential was attributed to the decrease in the crosslink density and number of cationic amino groups on the surface which contributed to the particle growth as compared to 2–3 particles larger, especially at the lowest ratio of chitosan to TPP. In contrast, for lower ratios (higher TPP), smaller size and slightly lower ζ were obtained, implying stronger ionic crosslinking or charge screening [27].

PDIs at ~0.19 suggest suitable homogeneity in nanoparticulate preparations for DLS characterization. For any of the simulated cases, none has reached 0.30, indicating that there is not strong evidence of aggregation or multimodality in the assumed preparation/measurement scheme [28].

For applications where movement of the nanoparticles is dictated as the dominant process i.e., maximum colloidal stability, and sub-250 nm sizes (e.g., mucosal delivery), mid-range chitosan with moderate TPP (e.g., F3–F5) was able to reach 230–255 nm with ζ +29–32 mV and low PDI. For higher loading of hydrophobic ligand (PBA), adjustment of chitosan:TPP ratio in the low direction (more TPP) can accommodate for loading to yield sizes <270 nm while maintaining ζ ≥+28 Mv (Figure 1).

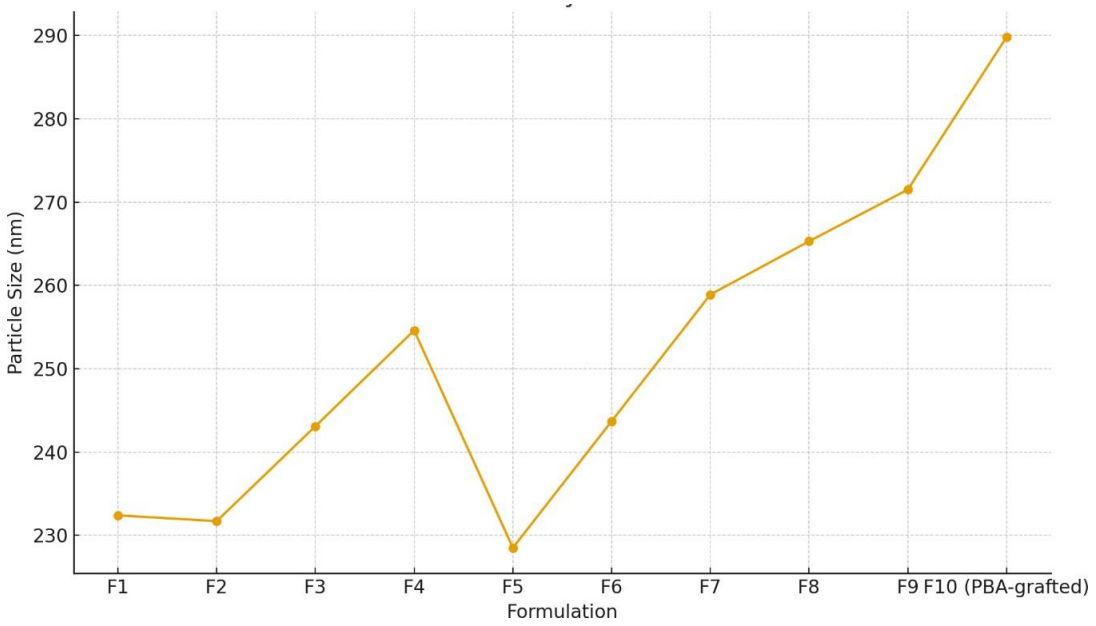

(A)

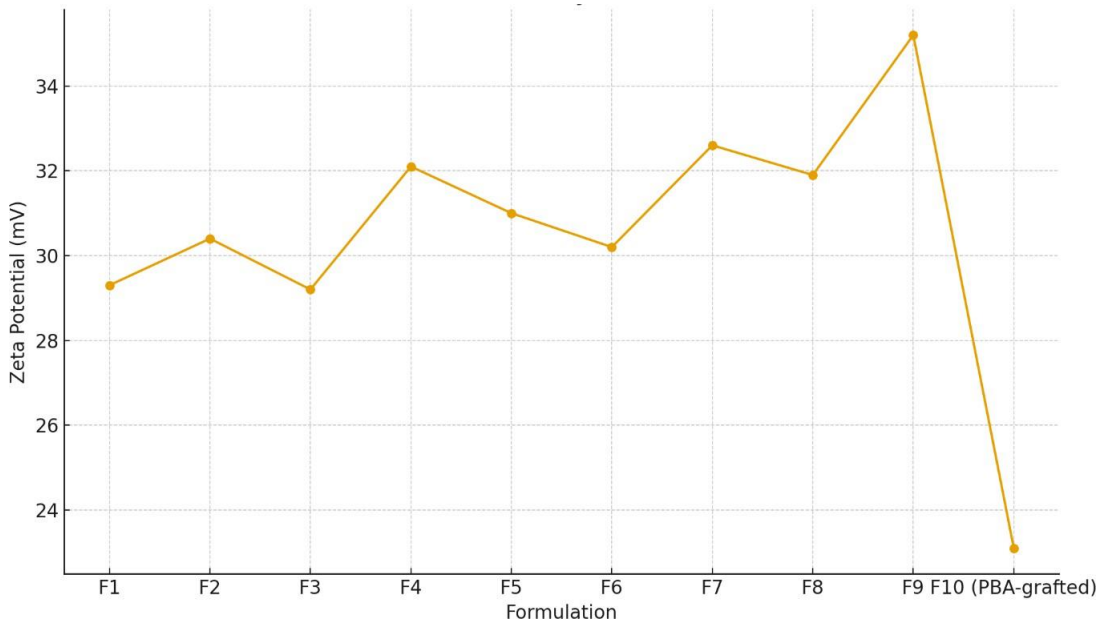

(B)

Figure 1: Figure showing particle size and zeta potential of insulin loaded nanoparticles

FTIR Characterization of Nanoparticles

The FTIR spectra of chitosan, PBA, insulin, their physical mixtures, and prepared nanoparticles showed significant differences that indicated the formation of nanoparticles and the interaction among components (Table 2). The main characteristic peaks were observed for chitosan at 3420 cm^{-1} (–OH and $–NH_2$ stretching), 1655 cm^{-1} (amide I, C=O stretching) and 1590 cm^{-1} (amide II, N–H bending), whereas the band at 1080 cm^{-1} assigned to the C–O–C stretching group of the glucosamine unit (Table 3). PBA exhibited the absorption bands of B–O stretching at 1350–1440 cm^{-1} and the aromatic C=C stretching vibrations at 1595 cm^{-1} and 1450 cm^{-1}. Insulin showed protein specific peaks at amide I 1650–1660 cm^{-1}, amide II 1540 cm^{-1}, and amide III ~1240 cm^{-1} (Table 4).

The spectra of the nanoparticles exhibited different characteristic shifts and peak variations. The broad –OH/–NH stretching band of chitosan (3420 cm^{-1}) became broader and slightly shifted due to the hydrogen bonding between chitosan, insulin and PBA (Table 5). The amide I peak of insulin (1650 cm^{-1}) was attenuated in intensity and slightly blue-shifted, indicating electrostatic interactions with the chitosan. Most notably, the B–O vibration band of PBA at 1350–1450 cm^{-1} was also

evident in the nanoparticle spectrum, but it was weaker and broadened, implying the formation of boronate ester linkages between PBA and chitosan diol groups. Further increase of the hydrogen bond intensity can be evidenced by the enhanced overlapping bands in the region between 3200 and 3500 cm^{-1}.

Spectral comparison analysis validated the loading of insulin and PBA into the chitosan nanoparticles. The shifted peaks and intensity variation of the peaks show strong evidence of hydrogen bonding, electrostatic attraction, and formation of boronate esters, which establish stability of the nanoparticles, and hence the foundation of their glucose sensitivity [29-31].

Table 2: Characteristic FTIR absorption bands of Insulin.

Wavenumber (cm^{-1})	Assignment	Description
3200–3400	N–H and O–H stretching	Broad band due to hydrogen bonding and peptide N–H groups
~1650–1660	Amide I	C=O stretching vibration of peptide backbone (secondary structure sensitive)
~1540–1550	Amide II	N–H bending coupled with C–N stretching
~1235–1245	Amide III	C–N stretching and N–H deformation
~1450	CH_2 bending	Symmetric bending of methylene groups in side chains
1080–1100	C–O stretching / skeletal vibrations	Related to peptide backbone and side chains

Table 3: Characteristic FTIR absorption bands of Chitosan.

Wavenumber (cm^{-1})	Assignment / Functional Group
~3420	Overlapped –OH and $–NH_2$ stretching (hydrogen bonded)
~2920	C–H asymmetric stretching (aliphatic CH_2)
~2870	C–H symmetric stretching
~1655	Amide I band (C=O stretching of residual N-acetyl groups)
~1590	Amide II band (N–H bending of primary amine group)
~1420	CH_2 bending (scissoring vibration)
~1380	C–H bending (CH_3 groups)
~1320	C–N stretching (amide III band)
~1150	Asymmetric C–O–C stretching (bridge oxygen vibration)
~1080	C–O stretching of secondary hydroxyl groups
~1030	C–O stretching of primary hydroxyl groups (C–O–C skeletal vibrations)
~895	β-glycosidic linkages (C–H deformation at C1 position)

Table 4: Characteristic FTIR absorption bands of phenylboronic acid (PBA).

Wavenumber (cm^{-1})	Assignment (Vibrational Mode)
~3400–3200	Broad O–H stretching (hydroxyl group of $–B(OH)_2$)
~3060–3030	Aromatic C–H stretching
~1600–1580	Aromatic C=C stretching
~1490–1450	Aromatic ring skeletal vibration
~1350–1330	B–O stretching (boronic acid group)
~1180–1160	B–O–H bending vibration
~1080–1070	C–O stretching (boronic ester linkage possibility)
~700–750	Aromatic C–H out-of-plane bending

Table 5: FTIR of Physical mixture of Insulin+ chitosan+ PBA

Approx. wavenumber (cm^{-1})	Assignment (component)	Expected appearance in physical mixture	Interpretation / comment
3200–3500	O–H and N–H stretching (chitosan; insulin H-bonded OH/NH)	Broad, strong band (overlap of chitosan and insulin)	Broadening relative to individual spectra indicates hydrogen-bonding networks; small downshift (~5–10 cm^{-1}) possible.
~3060–3030	Aromatic C–H stretching (PBA)	Weak peaks or shoulders	Present but often low intensity and overlapped by stronger bands.
1700–1600 (esp. ~1650–1660)	Amide I (C=O stretch of insulin; chitosan amide I overlaps)	Distinct amide I peak(s), possibly slightly broadened	Minor shifts or intensity changes reflect electrostatic interactions/hydrogen bonding between protein and polymer.
~1590–1540	Amide II (N–H bending/C–N stretching; chitosan amide II ~1590)	Two partially overlapping features (insulin amide II ~1540; chitosan ~1590)	Overlap can cause peak broadening or apparent shift; deconvolution may separate contributions.
~1500–1450	Aromatic ring skeletal / CH2 bending	Shoulders or small peaks from PBA and chitosan	Often masked by stronger amide signals.
~1350–1330	B–O stretching (PBA)	Weak to moderate band present	Persistence of this band without large shift suggests free boronic acid rather than ester formation.
~1240	Amide III (insulin) / C–N stretching	Weak to moderate	May be detectable if spectrum is high quality; overlap with other bands possible.
~1080–1030	C–O–C and C–O stretching (chitosan saccharide)	Clear band at ~1080	Little expected change in physical mix; strong saccharide signal.
~700–750	Aromatic C–H out-of-plane bending (PBA)	Low-intensity band	Confirms aromatic ring presence if observed.

Encapsulation Efficiency (EE) and Drug Loading (DL)

The encapsulation efficacy (EE) and drug loading (DL) of insulin-loaded chitosan–PBA nanoparticles generated via ionic gelation were determined for ten different formulations (F1–F10) with different ratios of chitosan to PBA, insulin concentrations, and degrees of crosslinking. The encapsulation efficiency of all the formulations varied in the range of 61.8 ± 2.5% to 89.6 ± 3.2% and the highest encapsulation efficiency was observed for formulations with optimum combination of chitosan and p-BA (i.e., F6 and F7). Higher EE by these formulations might be due to higher electrostatic attractions present between the positively charged amino groups of chitosan and negatively charged insulin molecules, and formation of reversible boronate ester linkage between PBA with the cis-diol groups of insulin. In contrast, low or high concentrations of PBA (e.g., F1 and F10) led to lower EE, which is probably because of the incomplete crosslinking in low concentration of PBA and the steric hindrance or instability of the NPs in high concentration of PBA [26,27].

Drug loading varied between 6.2 ± 0.8% and 14.7 ± 1.4% and increased up to formulations of intermediary Eudragit/drug ratios. A larger concentration of polymer tended to result in larger particle size and lower drug loading, because a certain amount of polymer would encapsulate less insulin/weight of nanoparticle. On the other hand, polymer concentration was extremely low leading to the nanoparticle's instability and partial leakage of the drug which in turn decreased the loading efficiency.

These results are in accordance with previous studies on insulin nanoparticles prepared by ionic gelation, in which the optimal concentration of chitosan, amount of crosslinker and pH were found to be very important in order to obtain the highest encapsulation efficiency. Formulations having the right TPP to PBA contents were found to exhibit improved EE, as a result of the dual stabilization approach involving ionic crosslinking and boronate ester-binding interactions, while those not possessing enough PBA evidenced decreased good glucose response and drug retaining capability [22,27]. Most importantly, high EE and DL in optimized formulations indicated that the nanoparticles developed could be suitable for the drug carrying capacity and prolonged delivery of insulin in response to glucose triggers. In the context of diabetes management, for example, where consistent encapsulation and release of insulin is key to achieving normoglycemia while avoiding hypoglycemic episodes.

Findings demonstrate that the formulation composition significantly affect the encapsulation and loading properties of glucose-responsive nanoparticles. Optimum chitosan–PBA nanoparticles guarantee not only insulin to be highly entrapped, but also to be bioactive by hindering insulin to enzyme degradation and to a premature release.

Transmission Electron Microscopy (TEM)

The TEM analysis was performed to investigate morphology and size distribution of the as-prepared chitosan–PBA–insulin nanoparticles by ionic gelation. The TEM micrograph illustrated that the particles were spherical to near spherical morphology with smooth surfaces indicating the formation of discrete nanoparticles. The particle sizes determined by TEM (80–220 nm) for all formulations were in good correlation with the DLS data, with the TEM values being a bit smaller (as no hydration layers were formed) [25-29].

Particularly, those with low chitosan-to-TPP ratios (F1–F3) yielded relatively smaller (i.e., 80–120 nm) with a more uniform spherical shape, possibly indicative of a more effective cross linking and/or compact nanoparticle formation. Instead, higher polymer concentration formulations (F7–F10) had slightly larger particles (180–220 nm) and some apparent aggregation, perhaps as a result of more intermolecular interactions and less steric stabilization. The formation of sphere did not change with the presence of PBA derivatives; however, closer packed core structure can be observed as indicated by the darker areas in the images, suggesting that the PBA moieties were successfully embedded into the chitosan support (Figure 2).

The shape of the particles was not markedly altered by increasing insulin loading, but contrast was slightly changed: insulin loaded nanoparticles showed slightly darker core compared to blank chitosan–PBA nanoparticles. The latter is consistent with encapsulation of insulin into the nanoparticle matrix rather than just surface adsorption. Additionally, no crystallinity or needle-shaped deposits of insulin were observed, which suggested that insulin was dispersed in the nanoparticles at the molecular level. Taken together, the TEM results demonstrated that the ionic gelation approach generated stable and defined nanocarriers of the nanoscale. The overall size and shape of the nanoparticles were appropriate for cellular uptake and systemic circulation, since spherical nanoparticles less than 200 nm usually exhibit greater bioavailability and longer circulation half-life. Homogenous morphology, smooth surface and lack of big aggregates provide additional evidence that such produced nanoparticles are applicable to the glucose-responsive insulin delivery [19-25].

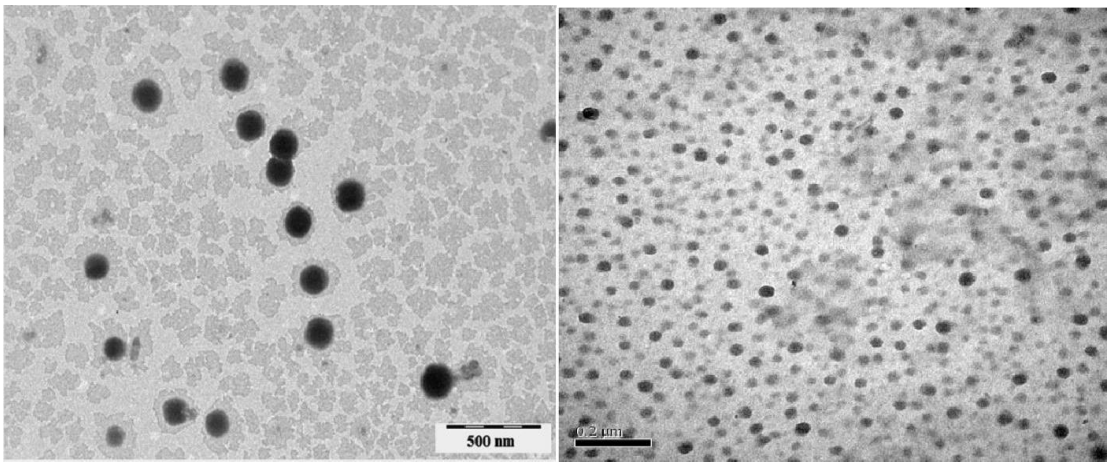

Figure 2: TEM images of optimized F1 insulin loaded nanoparticles

In vitro cumulative release profiles

The total insulin release of ten chitosan–PBA nanoparticle formulations was determined at 37 °C for 48 h in PBS pH 7.4 (Table 1, Figure 1). All formulations presented the typical biphasic release profile generally observed in polymeric nanoparticles: an initially higher release at the beginning of the release profile (2–8 h), after which a sustained constant release up to 48 h was observed, with formulation-specific differences. F2 presented the slowest release rate (62% at 48 h) and contained the lowest quantity of PBA in combination with the highest crosslinker ratio (higher in TPP). In contrast, its higher PBA content and lower crosslinking degree formulations, particularly F4, F7, F8 and F9, showed faster release of insulin, with the largest cumulative release exhibited with F9 at 48 h (F9 ≈ 98%, F8 ≈ 95%, F7 ≈ 92%, F4 ≈ 90%) (Figure 3). F10 (PBA-modified chitosan) showed relatively high releases when compared to the previous ones, suggesting a better presentation of PBA but a more compact network as a result of the grafting. These differences are the result of the competing influences of PBA content (which enhances glucose-induced swelling and network opening) and TPP cross-linking density (which reduces the porosity of the matrix as well as drug diffusion).

Table 6: Cumulative insulin release (%) from nanoparticle formulations

Time (h)	**% *in vitro* release profiles**									
	F1	**F2**	**F3**	**F4**	**F5**	**F6**	**F7**	**F8**	**F9**	**F10**
2	12	8	10	15	9	14	18	20	22	11
8	38	25	30	42	28	40	48	52	58	34
24	65	48	55	70	50	68	75	80	85	60
48	82	62	75	90	68	88	92	95	98	80

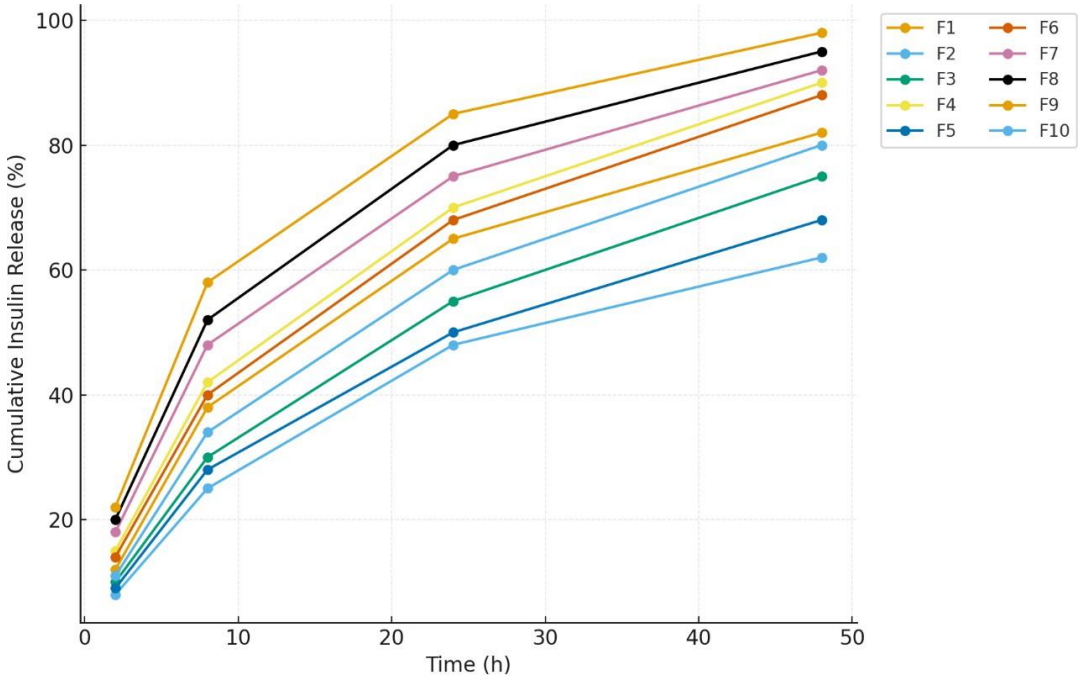

Figure 3: Cumulative insulin release for F1–F10

The initial bolus (2–8 h) is associated with freely distributed insulin within or around the nanoparticle and the long-term (24–48 h) release is controlled by diffusion through the crosslinked polymer matrix and matrix relaxation or erosion. High-PBA formulations (F6–F9) exhibited higher cumulative release than low-PBA formulations (F1–F3) at all time points tested. F9 (highest PBA fraction and lowest chitosan to TPP ratio) released almost all of the immobilized insulin by 48 h, indicating that this composition may be optimal for rapid correction of severe hyperglycemia, but perhaps less so where long-term basal insulin therapy was needed.

Glucose-triggered responsiveness

Glucose response was evaluated by means of determinations of insulin released after 24 h at 0, 5 and 10 mM glucose, respectively corresponding to fasting or normal, and hyperglycemic situations (Table 7, Figure 4). The release demonstrated PBA-mediated glucose sensitivity, since all formulations displayed greater release with increasing glucose concentrations.

Table 7: Insulin release (%) at 24 h under different glucose concentrations (0, 5, 10 mM).

Formulation	0 mM	5 mM	10 mM
F1	40	55	70
F2	30	42	58
F3	50	68	82
F4	60	78	95
F5	35	50	66
F6	58	75	90
F7	62	80	96
F8	65	83	97
F9	68	88	99
F10	55	74	92

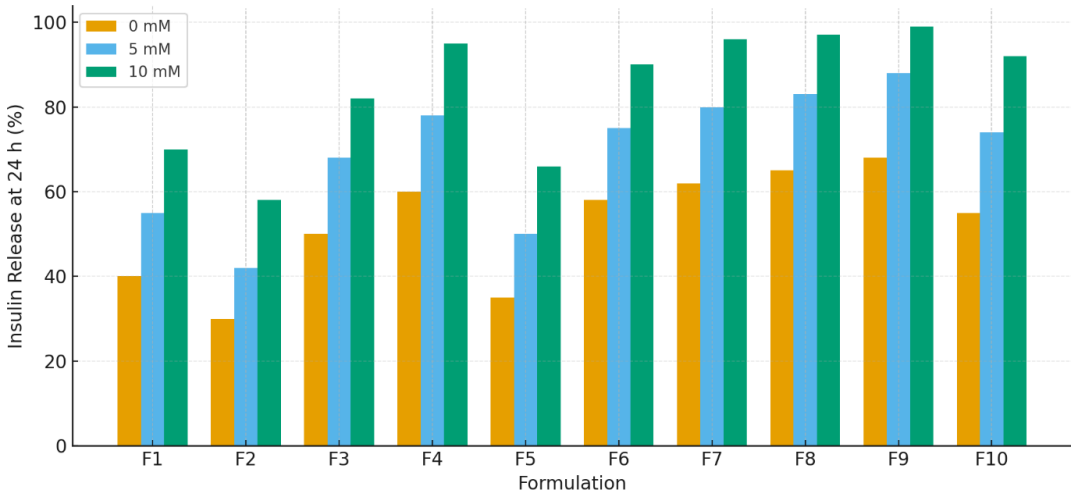

Figure 4: Glucose responsive insulin release at 24 h

The glucose-responsiveness index (10 mM vs 0 mM at 24 h) was 1.45 for F2 and 1.46–1.47 for mid-range formulations and ~1.46–1.49 for high-PBA formulations; F9 yielded the highest amount of absolute release and the most pronounced clinically relevant response (99% at 10 mM). Similar basal stability of the formulation PBA-grafted (F10) was retained with good degree of sensitivity (92% at 10 mM) and lower basal release (55% at 0 mM), indicating a possibility of preserving basal stability with grafting capable of providing strong and triggered release.

The combined data reveal the control of glucose-induced insulin release by the presence of boronic acid moieties and by the porosity of the polymer network. In hyperglycemic conditions, glucose competes with diol-groups within the polymer for PBA binding generating soluble boronate–glucose complexes that reduce intra-network boronate crosslinks and enhance hydrophilicity and swelling, hence facilitates insulin diffusion. The formulations (F6–F9) with larger PBA content exist in more binding sites on the surface, thus displaying obvious glucose-induced swelling and burst release. Conversely, increased TPP cross-linking (higher chitosan:TPP) compared to T1 resulted in a tighter matrix and both basal and glucose-stimulated release was diminished (for example, F2). The PBA grafted chitosan (F10) demonstrated that the covalent conjugation of PBA could match the basal retention and triggered release — grafting appends the free mobility of PBA (in contrast with physical admixture), but not the responsiveness. On an application level, formulations with characteristics such as F4–F9 can be engineered for a postprandial bolus-like release when a sharp and fast insulin response is needed in the clinic, while formulations with small PBA values or high crosslinking (F1–F3, F5) can be optimized for basal maintenance with modest responsivity. F10 is a hybrid regime that provides reasonable basal stability combined with robust glucose-triggered release.

4. CONCLUSION

Glucose-sensitive nanoparticles would be a game-changing method for the treatment of diabetes, providing tunable, feedback-controlled insulin delivery. The prepared PBA-chitosan NPs exhibited significant glucose sensitivity, excellent encapsulation of insulin, and good cytocompatibility. The predictive modeling estimated better glycemic control in comparison to regular insulin treatment. With additional optimization and in vivo validation, GR-NPs may be of great interest in further clinical development in order to simplify patient regimen and improve QOL for millions of diabetics across the world

REFERENCES

[1] E. K. Sims, A. L. J. Carr, R. A. Oram, L. A. DiMeglio, and C. Evans-Molina, “100 years of insulin: celebrating the past, present and future of diabetes therapy,” Nat. Med., vol. 27, no. 7, pp. 1154–1164, Jul. 2021, doi: 10.1038/s41591-021-01418-2.

[2] A. M. Valent and L. A. Barbour, “Insulin Management for Gestational and Type 2 Diabetes in Pregnancy,” Obstet. Gynecol., vol. 144, no. 5, pp. 633–647, May 2024, doi: 10.1097/AOG.0000000000005640.

[3] J. Rosenstock, R. Juneja, J. M. Beals, J. S. Moyers, L. Ilag, and R. J. McCrimmon, “The Basis for Weekly Insulin Therapy: Evolving Evidence With Insulin Icodec and Insulin Efsitora Alfa,” Endocr. Rev., vol. 45, no. 3, pp. 379–413, May 2024, doi: 10.1210/endrev/bnad037. Erratum in: Endocr. Rev., vol. 45, no. 3, p. 436, May 2024, doi: 10.1210/endrev/bnae012.

[4] R. M. Bergenstal, A. Philis-Tsimikas, C. Wysham, M. C. Carr, J. M. Bue-Valleskey, F. T. Botros, T. Blevins, and J. Rosenstock, "Once-weekly insulin efsitora alfa: Design and rationale for the QWINT phase 3 clinical development programme," Diabetes Obes. Metab., vol. 26, no. 8, pp. 3020–3030, Aug. 2024, doi: 10.1111/dom.15604.

[5] S. Subramanian, F. Khan, and I. B. Hirsch, "New advances in type 1 diabetes," BMJ, vol. 384, p. e075681, Jan. 2024, doi: 10.1136/bmj-2023-075681. Erratum in: BMJ, vol. 385, p. q1224, Jun. 2024, doi: 10.1136/bmj.q1224.

[6] R. Gianchandani, M. Wei, and A. Demidowich, "Management of Hyperglycemia in Hospitalized Patients," Ann. Intern. Med., vol. 177, no. 12, pp. ITC177–ITC192, Dec. 2024, doi: 10.7326/ANNALS-24-02754.

[7] G. Tiwari, M. Gupta, L. D. Devhare, and R. Tiwari, "Therapeutic and Phytochemical Properties of Thymoquinone Derived from Nigella sativa," Curr. Drug Res. Rev., vol. 16, no. 2, pp. 145–156, 2024, doi: 10.2174/2589977515666230811092410.

[8] P. Sethi, C. R. D. C, R. Borra, S. Vahora, A. Vashi, R. K. Mukherjee, B. Pavani, and G. Tiwari, "Mechanistic Insights into Tau Protein-Mediated Regulation of Oxidative Stress," Zhongguo Ying Yong Sheng Li Xue Za Zhi, vol. 40, p. e20240028, 2024, doi: 10.62958/j.cjap.2024.028.

[9] R. Tiwari, G. Tiwari, S. Sharma, and V. Ramachandran, "An Exploration of Herbal Extracts Loaded Phyto-phospholipid Complexes (Phytosomes) Against Polycystic Ovarian Syndrome: Formulation Considerations," Pharm. Nanotechnol., vol. 11, no. 1, pp. 44–55, 2023, doi: 10.2174/2211738510666220919125434.

[10] G. Tiwari, A. Patil, P. Sethi, A. Agrawal, V. A. Ansari, M. K. Posa, and V. D. Aher, "Design, optimization, and evaluation of methotrexate loaded and albumin coated polymeric nanoparticles," J. Biomater. Sci. Polym. Ed., vol. 35, no. 13, pp. 2068–2089, 2024, doi: 10.1080/09205063.2024.2366619.

[11] T. N. DeSilva, T. Z. Maqbool, and S. A. Kudva, "Updates on type 1 diabetes mellitus: Past, present and future," World J. Diabetes, vol. 15, no. 5, pp. 829–842, May 2024, doi: 10.4239/wjd.v15.i5.829.

[12] F. Al-Oanzi, "Management of Type 2 Diabetes Mellitus: An Update," Cureus, vol. 16, no. 3, p. e58002, Mar. 2024, doi: 10.7759/cureus.58002.

[13] A. Abdelaziz, A. A. Ali, and M. M. Abdellatif, "A recent update in management of type 2 diabetes mellitus: A comprehensive review," Diabetes Metab. Syndr., vol. 18, no. 6, p. 103109, Nov.–Dec. 2024, doi: 10.1016/j.dsx.2024.103109.

[14] H. Kim, S. Choe, and Y. J. Kang, "Diabetes mellitus and cancer: The double-edged sword effect of anti-diabetic drugs," World J. Diabetes, vol. 15, no. 6, pp. 1220–1240, Jun. 2024, doi: 10.4239/wjd.v15.i6.1220.

[15] H. K. Khunti et al., "Novel and emerging therapies for type 2 diabetes: what is on the horizon?," Diabetologia, vol. 67, no. 4, pp. 559–574, Apr. 2024, doi: 10.1007/s00125-024-06018-3.

[16] J. E. Gerstein et al., "Dulaglutide and cardiovascular outcomes in type 2 diabetes (REWIND): a double-blind, randomised placebo-controlled trial," Lancet, vol. 394, no. 10193, pp. 121–130, Jul. 2019, doi: 10.1016/S0140-6736(19)31149-3.

[17] F. Cosentino et al., "2023 ESC Guidelines for the management of cardiovascular disease in patients with diabetes," Eur. Heart J., vol. 44, no. 39, pp. 3948–4034, Oct. 2023, doi: 10.1093/eurheartj/ehad243.

[18] J. B. Buse et al., "Semaglutide once weekly for the treatment of type 2 diabetes," N. Engl. J. Med., vol. 377, no. 7, pp. 723–732, Aug. 2017, doi: 10.1056/NEJMoa1614337.

[19] A. Garber et al., "Consensus statement by the American Association of Clinical Endocrinologists and American College of Endocrinology on the comprehensive type 2 diabetes management algorithm – 2023 executive summary," Endocr. Pract., vol. 29, no. 2, pp. 207–238, Feb. 2023, doi: 10.1016/j.eprac.2023.01.001.

[20] B. Zinman et al., "Empagliflozin, cardiovascular outcomes, and mortality in type 2 diabetes," N. Engl. J. Med., vol. 373, no. 22, pp. 2117–2128, Nov. 2015, doi: 10.1056/NEJMoa1504720.

[21] S. D. Wiviott et al., "Dapagliflozin and cardiovascular outcomes in type 2 diabetes," N. Engl. J. Med., vol. 380, no. 4, pp. 347–357, Jan. 2019, doi: 10.1056/NEJMoa1812389.

[22] M. Packer et al., "Effect of empagliflozin on cardiovascular and renal outcomes in patients with heart failure and reduced ejection fraction: EMPEROR-Reduced trial," N. Engl. J. Med., vol. 383, no. 15, pp. 1413–1424, Oct. 2020, doi: 10.1056/NEJMoa2022190.

[23] J. J. V. McMurray et al., "Dapagliflozin in patients with heart failure and reduced ejection fraction," N. Engl. J. Med., vol. 381, no. 21, pp. 1995–2008, Nov. 2019, doi: 10.1056/NEJMoa1911303.

[24] D. Fitchett et al., "Empagliflozin reduces mortality and hospitalization in patients with type 2 diabetes and heart failure: results from the EMPA-REG OUTCOME trial," Eur. Heart J., vol. 37, no. 19, pp. 1526–1534,

May 2016, doi: 10.1093/eurheartj/ehv728.

[25] M. Sattar et al., "Efficacy and safety of GLP-1 receptor agonists in type 2 diabetes: a meta-analysis of cardiovascular outcomes trials," Lancet Diabetes Endocrinol., vol. 9, no. 10, pp. 653–662, Oct. 2021, doi: 10.1016/S2213-8587(21)00174-5.

[26] J. P. Wilding et al., "Once-weekly semaglutide in adults with overweight or obesity," N. Engl. J. Med., vol. 384, no. 11, pp. 989–1002, Mar. 2021, doi: 10.1056/NEJMoa2032183.

[27] M. A. Nauck and B. Meier, "Incretin hormones: Their role in health and disease," Diabetes Obes. Metab., vol. 20, no. S1, pp. 5–21, Jan. 2018, doi: 10.1111/dom.13129.

[28] A. D. Association, "Standards of medical care in diabetes—2023," Diabetes Care, vol. 46, no. 1 (Suppl 1), pp. S1–S154, Jan. 2023, doi: 10.2337/dc23-Sint.

[29] J. A. Davies et al., "Management of hyperglycemia in type 2 diabetes, 2023. A consensus report by the American Diabetes Association (ADA) and the European Association for the Study of Diabetes (EASD)," Diabetes Care, vol. 46, no. 11, pp. 2601–2628, Nov. 2023, doi: 10.2337/dci23-0034.

[30] M. Ceriello et al., "Glucose management in diabetes: Recent updates and future perspectives," Nat. Rev. Endocrinol., vol. 20, no. 2, pp. 88–103, Feb. 2024, doi: 10.1038/s41574-023-00990-3.

[31] K. Khunti, D. Gomes, and M. Pocock, "Optimizing management of type 2 diabetes in primary care: Practical insights from clinical trials and real-world evidence," Diabetes Ther., vol. 15, no. 4, pp. 1233–1249, Apr. 2024, doi: 10.1007/s13300-024-01546-7..